Microstructural evolution characterization of Fe-Nb-B ternary systems processed by ball milling

J. J Ipus, Javier Sebastián Blázquez, Sergio Lozano-Perez, Alejandro Conde

Microstructural evolution characterization of Fe-Nb-B ternary systems processed by ball milling

Journal:	*Philosophical Magazine & Philosophical Magazine Letters*
Manuscript ID:	TPHM-09-Feb-0047.R1
Journal Selection:	Philosophical Magazine
Date Submitted by the Author:	31-Mar-2009
Complete List of Authors:	Ipus, J.; Sevilla University, Física de la Materia Condensada Blázquez, Javier; Sevilla University, Física de la Materia Condensada Lozano-Perez, Sergio; University of Oxford, Materials Conde, Alejandro; Sevilla University, Física de la Materia Condensada
Keywords:	amorphous alloys, ball-milling, FIB, nanocrystals, TEM
Keywords (user supplied):	amorphous alloys, ball-milling, FIB

Microstructural evolution characterization of Fe-Nb-B ternary systems processed by ball milling

Jhon J. Ipus[1], Javier S. Blázquez[1], Sergio Lozano-Perez[2], Alejandro Conde[1]*

[1] Departamento de Física de la Materia Condensada, ICMSE-CSIC, Universidad de Sevilla, P.O. Box 1065, 41080, Sevilla, Spain.

[2] Department of Materials, University of Oxford, Parks Road, Oxford OX1 3PH, UK.

ABSTRACT: Fe-Nb-B alloys prepared by ball milling can undertake a complex microstructural evolution during milling. In order to overcome the limitations imposed by traditional X-ray bulk analysis, a comprehensive multi-technique approach was devised to systematically characterize samples with the required resolution. The combination of in-situ FIB (Focused ion beam) lift out and high resolution ATEM (Analytical transmission electron microscopy), have allowed the characterization of the phase evolution during milling. In particular, boron inclusions, not detected by X-ray diffraction, have been found to remain undissolved in the Fe matrix.

KEYWORDS: Ball milling, nanocrystalline alloys, amorphous alloys, FIB, TEM.

*Corresponding author: Prof. A. Conde

Departamento de Física de la Materia Condensada. Universidad de Sevilla.

Apartado 1065, 41080 Sevilla (Spain).

Phone: (34) 95 455 28 85/ Fax: (34) 95 461 20 97

E-mail: conde@us.es

Introduction

Fe based amorphous and nanocrystalline alloys are very interesting due to their magnetic properties [1], which are strongly linked with their metastable microstructure [2]. Mechanical alloying by ball milling has been shown as a very suitable and versatile technique in the production of both amorphous and nanocrystalline alloys in wide compositional ranges [3]. Generally, mechanical alloying is developed from a starting mixture of pure powders, which progressively become alloyed to form an amorphous and/or a supersaturated solid solution. The study of microstructural evolution is frequently followed by X-ray diffraction (XRD) [3,4,5,6,7,8,9], characterizing the phase evolution, average values of microstructural parameters (grain size and microstrains) and compositional information derived from evolution of the average lattice parameter. However, transmission electron microscopy (TEM) studies on ball milled powder samples are not so abundant (especially for magnetic materials) [4,8,10,11,12,13,14] due to the difficulties associated with sample preparation. TEM imaging and microanalysis supply local microstructural and compositional information overcoming the limitations of XRD. This is of special interest for the detection of minoritary phases (not only due to small volume fraction but also to low scattering power).

In this study, selected samples of Fe-Nb-B alloys prepared by ball milling were studied by different TEM imaging, diffraction and microanalysis techniques in order to obtain complementary information on the microstructure previously studied by XRD and Mössbauer spectrometry [15].

Experimental

$Fe_{100-x-y}Nb_xB_y$ (x=5, y=10 and x=10, y=15) compositions were prepared from elemental powders by ball milling in a planetary mill Fritsch Pulverisette 4 Vario. from elemental powders (>99% purity). The initial powder mass was 30 g and the ball to powder ratio was 10:1. Hardened steel balls were used with a composition 86 at. % Fe and 14 at. % Cr. The rotational speed of the disk which supports the vials was 150 rpm and that of the vials was 300 rpm in the opposite direction. The opening and closing of the vials were done under argon atmosphere in a Saffron Omega glove box to avoid oxygen and humidity contamination. For simplicity, the studied alloys will be named in the following by their Nb content: Nb10 for $Fe_{75}Nb_{10}B_{15}$ and Nb5 for $Fe_{85}Nb_5B_{10}$. Scanning electron microscopy (SEM) images obtained for short milling times show an initial mixture of the constituent elements forming heterogeneous powder particles [15]. In that previous study, evolution of the powder during milling process indicates that the maximum compositional homogenization was achieved after 50 h under the milling conditions used. However, dispersion on composition persists being constant up to the maximum explored milling time (400 h). The ratio between Fe and Fe+Nb content after 50 h milling is 90 ± 4 % and 95 ± 8 % for Nb10 and Nb5, respectively. Contamination from milling media yields the incorporation of Cr to the powder (1.8 and 0.6 at. % Cr for Nb10 and Nb5, respectively) [15].

Different electron microscopy techniques were used in this study, including transmission (TEM), scanning transmission (STEM) and high resolution electron microscopy (HREM). Conventional bright field (BF) and dark field (DF) were used, as well as high angle annular dark field (HAADF) in STEM mode. In diffraction mode, selected area diffraction (SAD) and convergent beam electron diffraction (CBED) patterns were acquired in order to identify the different phases. Several analytical techniques were used, including energy dispersive X-ray spectroscopy (EDX), using an

Oxford Instruments EDS ultra-thin window detector running Inca software, capable of a resolution of 137 eV for the Mn K α peak; electron energy loss spectroscopy (EELS) and energy filtered transmission electron microscopy (EFTEM) using a Gatan Image Filter (GIF) which provided an energy resolution of ~ 1eV. Experiments were performed using three different microscopes: a Philips CM-20 operated at 200 kV, a Philips CM200 operated at 200 kV and a Jeol JEM3000F operated at 297 kV.

Sample preparation

The preparation of TEM specimens was performed using a FIB FEI 200, following the lift out procedure [16,17,18,19], applied to individual powder particles. The procedure to prepare TEM samples using FIB is schematically shown in figure 1 for a typical powder sample. The main steps followed are:

- A protective Pt layer is deposited on the surface of a selected powder particle to prevent Ga^+ damage in the region of interest during cutting and thinning processes.
- A slice of approximately 15 µm x 5 µm x 2 µm is cut from the powder particle (figure 1a-b) and welded with the help of an in-situ micromanipulator (figure 1c) to a dedicated Cu grid for TEM examination (figure 1d).
- Finally, the TEM sample is thinned to electron transparency (figure 1e-f).

Results and Discussion

Figure 2 shows BF TEM images for Nb10 alloy after 50 h milling and both alloys after 400 h milling together with a SAD pattern of the former sample. The

observed microstructure for the Nb10 alloy after 50 h consists on a majority of nanocrystals with regular shape and average crystal size <D> ~10 nm (bcc-Fe type from SAD patterns in agreement with XRD results [15]). In particular, long shaped nanocrystals (Nb rich as it will be shown later in EDX maps) and larger bright inclusions in BF images (size ~100 nm) are randomly dispersed throughout the sample. For both alloys after 400 h milling, long shaped nanocrystals do not appear and the α-Fe type nanocrystals present a smaller average crystal size, <D> ~7 nm, than that of Nb10 after 50 h milling (this agrees with XRD results, where the crystal size is just slightly reduced after 50 h milling for both alloys). Moreover, large bright inclusions (smaller than for 50 h milling) are also observed. These inclusions exhibit a very weak contrast with respect to the holes in the samples, looking very bright in BF images (sometimes even saturating the negative when contrast in the nanocrystalline matrix is obtained). The brightness of these crystals in BF images could be ascribed to a low power scattering of the constituent elements of the crystals, characteristic of light elements as B, which is present in the studied alloys. Diffraction analysis evidences their crystalline nature and, moreover, lattice periodicity can be observed in HREM images.

Figure 3 (up right) shows a HREM image of one of these crystalline inclusions (up left) found in Nb5 after 400 h. Two interplanar spacings were measured with characteristic distances of d_{hkl}=0.55 nm and 0.42 nm and an angle of ~90º. Information about crystalline structure of these crystalline inclusions can be also obtained by convergent beam electron diffraction (CBED) patterns. As an example, figure 3 (down) shows a CBED pattern on a crystalline inclusion of the Nb5 alloy after 400 h. Interplanar distances of 5.2 Å and 3.6 Å were measured with an angle between them of 91º. B powder used in the initial mixture was characterized by X-ray diffraction and found to be β-B (JCPDF 00-031-0207). However, this phase is not consistent with the

CBED and HREM results. Pure B can exhibit several allotropic structures at room temperature and, amongst them, a tetragonal structure with lattice parameters $a = b = 8.57$ Å and $c = 8.13$ Å [20] which is a plausible solution for indexing both HREM images and CBED patterns. EELS analysis suggests that some carbon was incorporated to the particle during processing (carbon contamination is an usual occurrence during ball milling using steel balls), and might explain the different crystallographic phase observed.

In addition to microstructural characterization, chemical analyses were performed for the studied samples. Figure 4 shows EDX compositional maps for the three studied samples. For all the samples, a HAADF image is shown for identification of the different regions and individual maps of Fe, Nb and Cr (due to contamination from milling media [15]). In the case of Nb5 after 400 h milling image, the Pt layer deposited during FIB sample preparation is observed and EDX map of this element (not shown) evidences the sharp edge between this layer and the region of interest of the sample studied. The elemental maps have been equalized in order to enhance individual elemental contributions. For Nb10 alloy after 50 h milling, Fe and Nb are not completely mixed. The matrix formed by regular shaped nanocrystals is Fe rich and the long shaped crystals are identified as Nb rich particles. Moreover, Fe and Nb (and even Cr) free regions are observed in the EDX maps, corresponding to the bright inclusions in BF images and confirming its mainly pure B character (see corresponding HAADF image). In fact, X-rays emitted by B atoms have very low energy and cannot be efficiently detected by EDX. Besides Fe and Nb and, as expected from previous results [15], EDX maps show the presence of Cr in the alloy due to contamination from grinding media as Cr rich clusters. It is worth mentioning the Cr-contrast between this

Cr-rich cluster and the matrix, which indicates a very low Cr content in agreement with previous EDX experiments performed in SEM (below 1 at.% after 50 h milling) [15].

Compositional maps for both alloys after 400 h milling do not show independent Fe or Nb rich regions but both elements are homogeneously dispersed throughout the samples except for those regions where Fe and Nb are not detected, ascribed to B crystals. Hence, the milling process used is unable to completely incorporate the B into the Fe(Nb) rich matrix. B crystals were present since the starting mixture, although ~~(~~in a different crystalline structure, and remain for the length of the milling time explored in this study, although its size decreases from 50 to 400 h. With the milling time, homogeneous Cr content of the matrix increases in agreement with SEM results [15] and Cr cluster are not so well defined as for the sample milled 50 h.

In order to confirm the B composition of the bright inclusions in BF images, EELS and EFTEM experiments were performed. Figure 5 (up) shows the B content corresponding to the line profile drawn on the HAADF image obtained for Nb10 after 400 h milling. As the image provides Z-contrast, the B rich inclusion appears dark and the Fe(Nb) rich matrix appears brighter. In the inclusions, B signal is high and outside the inclusions is negligible. Figure 5 (down) shows EFTEM images for Nb5 after 400 h milling filtered for B and Fe energies, respectively, along with the corresponding BF image for comparison. The B rich inclusion (left hand) and the Fe rich nanocrystalline matrix (right hand) can be clearly distinguished.

The observed B crystalline phase in this study by TEM was not detected using XRD in previous studies on the same samples [15] because of the low scattering factor of B atoms. In fact, several authors studying Fe-X-B (X=Nb, Zr,…) systems achieve a final microstructure by ball milling consisting on amorphous and/or supersaturated solid solution nanocrystals without mentioning any B rich phase [6,7,9]. On the other hand,

Liu et al [11] detected B_2O_3 phase in Fe(Co,Ni)ZrB system submitted to ball milling. In the present study, EELS experiments do not show any significant oxygen in the B inclusions, discarding this oxide in the systems studied in this paper.

The evolution of Nb during ball milling is typical for ductile materials [3,21], developing long crystals with a large surface, which facilitates the incorporation of this element into the Fe nanocrystalline matrix forming a supersaturated α-Fe(Nb) solid solution. The present results do not disagree with the preferential partitioning of Nb to intercrystalline region derived from Mössbauer results [15]. In fact, the resolution of the microscopic technique used and the sample thickness prevent any conclusion at scales below ~1 nm (intercrystalline region).

The evolution of B during ball milling is typical for brittle materials [3], forming inclusions which, in this case, can not be incorporated into the Fe(Nb) supersaturated solid solution. It is worth mentioning that B compounds as BN and B_4C are among the harder materials known.

It is worth mentioning that using conventional XRD techniques, stationary state of the milled powder would be achieved after 50 h milling [15]. At such a time, no further evolution was detected for Nb5 alloy and a supersaturated solid solution is formed as the stationary phase. In the case of Nb10 alloy, a progressive amorphization is detected as milling progresses from 50 to 400 h, but without change in the global composition distribution of the powder particles (except for the contamination effects). Extrapolation of crystalline volume fraction dependence on milling time to very long times leads to a saturation value for crystalline fraction of ~10 %. However, very long milling could imply recrystallization processes [22]. Results obtained in the present work show that even far beyond the time considered for stationary state using global techniques B inclusions are detected.

Conclusions

The combination of different diffraction, imaging and analytical TEM techniques has allowed the characterization of the microstructural evolution of ball milled Fe-Nb-B alloys. While Nb and Fe followed the expected evolution during the milling process, B was found to remain undissolved for long milling times. This behavior, undetected by conventional X-ray diffraction analysis, is crucial to understand the evolution of the microstructure, the level of amorphization of the Fe matrix and some physical properties.

Acknowledgements

This work was supported by MEC of the Spanish Government and EU FEDER (Project MAT2007-65227) and the PAI of the regional Government of Andalucía (Project P06-FQM-01823). The TEM investigations were supported by the IP3 project of the 6th Framework Programme of the European Commission: ESTEEM Contract number 026019. J.J.I. acknowledges a fellowship from the Spanish Ministry of Education and Science. J.S.B. acknowledges a research contract from this Regional Government.

Figure captions

Figure 1. Images of the TEM sample preparation using FIB. In situ images from secondary electrons: a) and b) cutting of a powder particle after Pt layer deposition, c) sample welded to the micromanipulator, d) sample welded to the TEM sample holder and cut from the manipulator (marker length 10 μm) and e) sample thinned (marker length 2 μm). Finally, f) TEM BF image of the Nb10 after 50 h milling sample showing B inclusions.

Figure 2. From left to right SAD image of Nb10 after 50 h milling and BF TEM images of Nb10 after 50 h milling, Nb10 after 400 h milling and Nb5 after 400 h milling. The scale bar is common to the three BF images.

Figure 3. (up left): BF image of Nb5 after 400h showing a B inclusion and the Pt layer, (up right) HREM of this B inclusion, (down) CBED pattern of a B rich inclusion obtained for Nb5 alloy after 400 h milling and plausible indexation using a tetragonal crystalline structure with a=0.857 and c=0.813 nm corresponding to a [1 1 1] zone axis were (-1 0 1) with d=0.5898 nm and (-1 2 -1) with d=0.3467 nm form an angle of 91.77º.

Figure 4. HAADF image and EDX maps of Nb10 alloy after 50h milling (left column), Nb10 alloy after 400h milling (center column) and Nb5 alloy after 400h milling (right column) using K line for Fe, K plus L lines for Nb and K line for Cr. The Pt layer deposited during TEM sample preparation is indicated in the latter column.

Figure 5. (up) HAADF image of Nb10 alloy after 400h and B profile corresponding to the line drawn in the image obtained by EELS. (down) BF image and EFTEM images acquired at the characteristic energies of B and Fe of Nb5 alloy after 400h showing a B inclusion (left in the image), the nanocrystalline matrix (right in the image) and the Pt protective layer (below in the image).

References

[1]M.E. McHenry, M.A. Willard, D.E. Laughling, Prog. Mat. Sci. 44 (1999) 291-433.

[2]A. Hernando, M. Vázquez, T. Kulik, C. Prado, Phys. Rev. B 51 (1995) 3581- 3586.

[3] C. Suryanarayana, Prog. Mat. Sci. 46 (2001) 1-184.

[4] J. Y. Yang, T. J. Zhang, K. Cui, X. G. Li, J. Zhang, J. All. Compd. 242 (1996) 153-156.

[5] M. Sherif El-Eskandarany, A.A. Bahgat, N.S. Gomaa, N.A. Eissa J. All. Compd. 290 (1999) 181-190.

[6] J.J. Suñol, A. Gonzalez, J. Saurina, Ll. Escoda, P. Bruna, Mater. Sci. Eng. A 375-377 (2004) 874-880.

[7] W. Lu, L. Yang, B. Yan, W. Huang, B. Lu, J. All. Compd. 413 (2006) 85-89.

[8] Y. J. Liu, I. T. H. Chang, Mater. Sci. Eng. A 325 (2002) 25-30.

[9] A. Grabias, M. Kopcewicz, D. Oleszak, J. All. Compd. 339 (2002) 221-229.

[10] A. Bollero, B. Gebel, O. Gutfleisch, K. H. Müller, L. Schultz, P. J. McGuiness, G. Drazic, S. Kobe, J. All. Compd. 315 (2001) 243-250.

[11] Y. J. Liu, I. T. H. Chang, Mater. Sci. Eng. A 375-377 (2004) 1092-1096.

[12] S. W. Du, R. V. Ramanujan, J. Mag. Mag. Mat. 292 (2005) 286-298.

[13] S. Gang, H. Lianxi, W. Erde, J. Mag. Mag. Mat. 301 (2006) 319-324.

[14] J. Han, S. Lui, X. Zang, H. Du, C. Wang, Y. Yang, M. Yue, X. Liu, J. Appl. Phys. 101 (2007) 09K502.

[15] J. J. Ipus, J. S. Blázquez, V. Franco, A. Conde, Intermetallics 16 (2008) 1073-1082.

[16] B. I. Prenitzer, L. A. Giannuzzi , K. Newman , S. R. Brown , R. B. Irwin , T. L. Shofner , F. A. Stevie, Met. Mat. Trans. A: Phys. Met. Mat. Sci. 29 (1998) 2399-2406.

[17] J. M. Carney, P. R. Munroe, Mat. Char. 46 (2001) 297-304.

[18] Y. Fujikawa, F. Yamane, T. Nomura, Y. Kitano, Ceram. Trans. 150 (2004) 115-123.

[19] S. Lozano-Perez, Micron 39 (2008) 320-328.

[20] A. Taylor, B. J. Kagle (1963). Crystallographic data on metal and alloy structures, p. 254, New York, USA: Dover.

[21] R.M. Davis, B. McDermott, C.C. Koch, Metall. Trans. A. 19 (1988) 2867-2873.

[22] S. Sharma, C. Suryanarayana, J. Appl. Phys. 102 (2007) 083544.

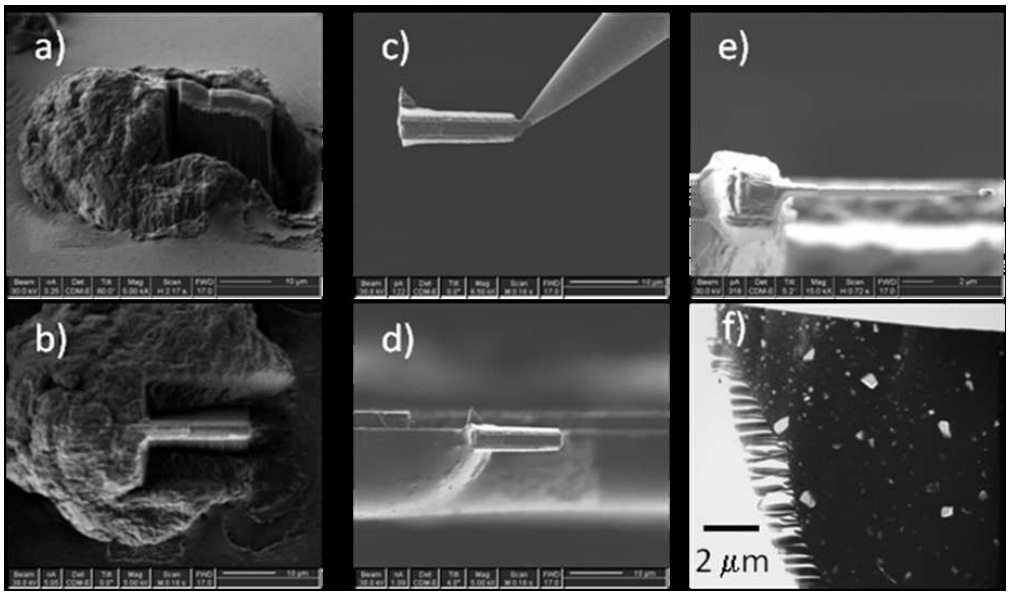

156x92mm (150 x 148 DPI)

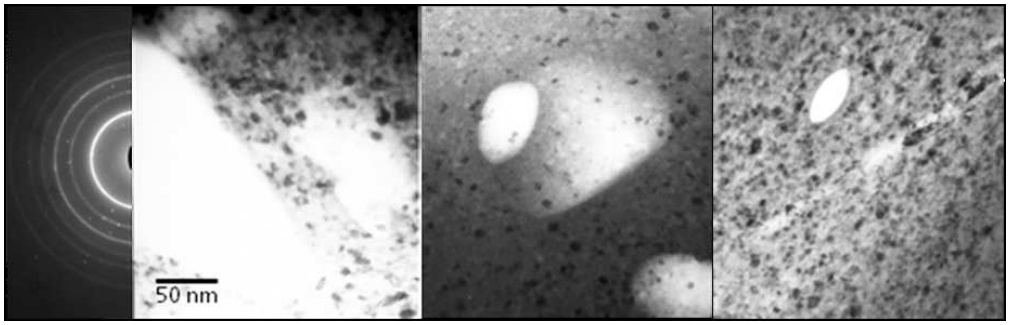

156x50mm (150 x 148 DPI)

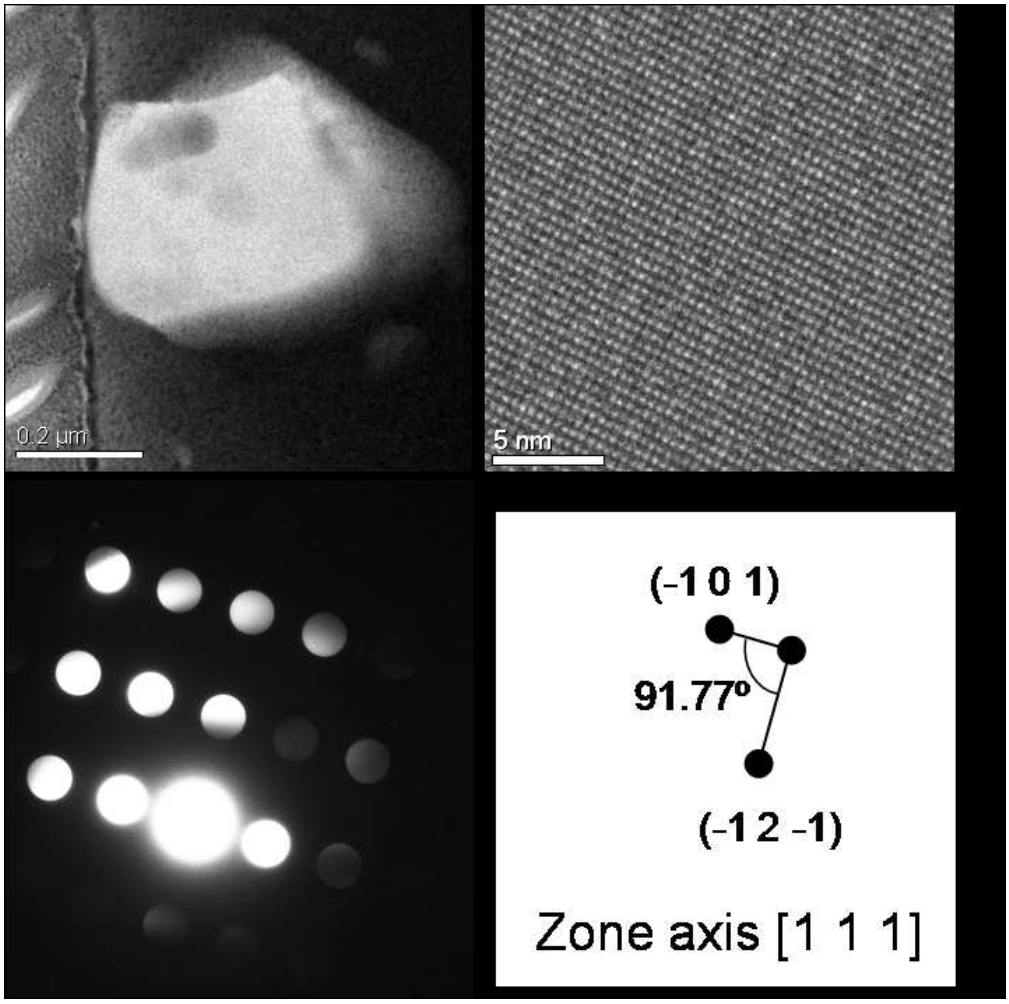

121x120mm (150 x 150 DPI)

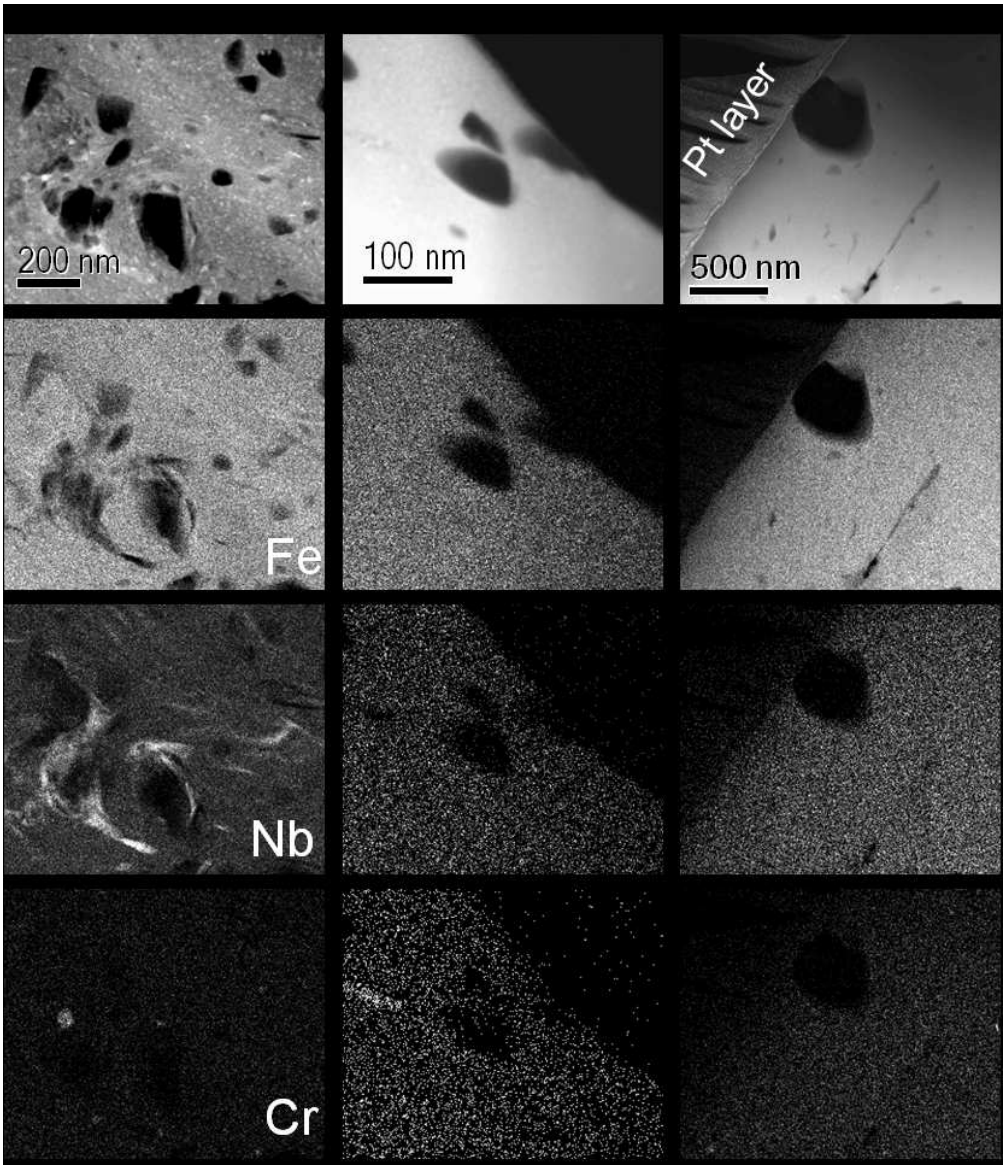

140x163mm (150 x 150 DPI)

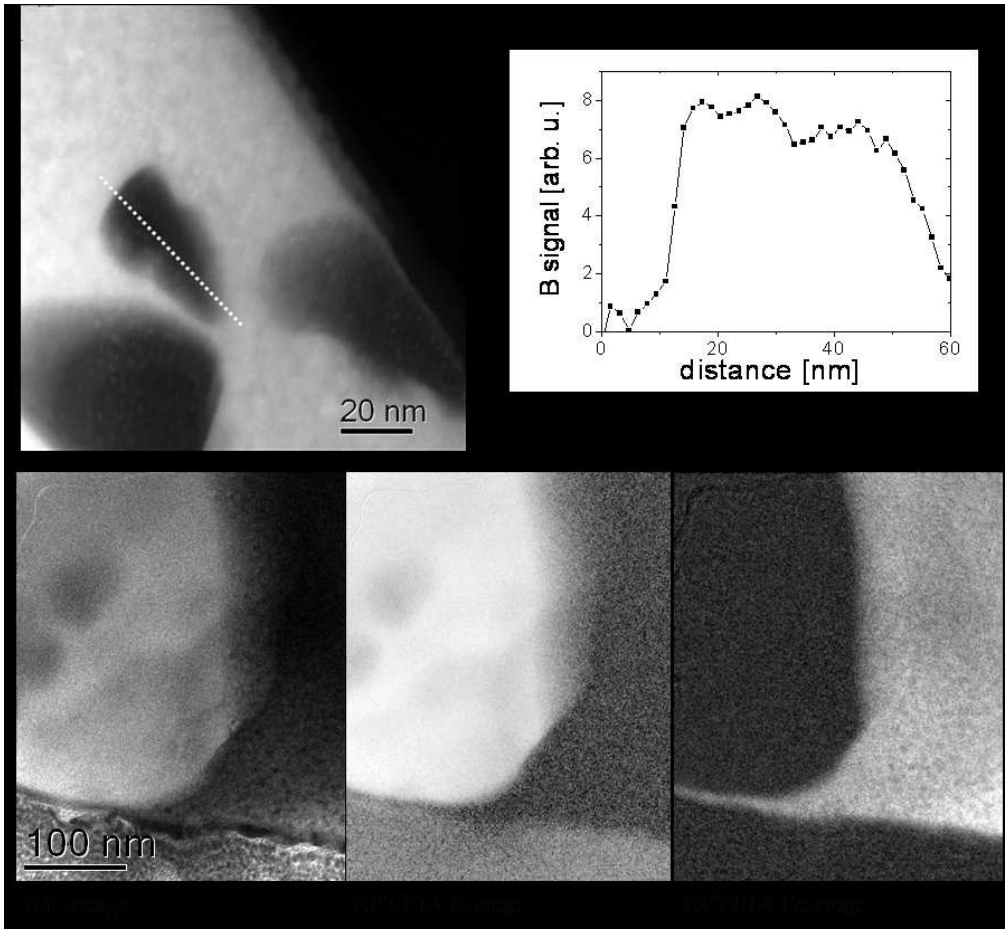

151x140mm (150 x 150 DPI)